

PACS numbers: 61.05.Cm, 61.80.Jh, 73.61.Ey, 74.62. Yb

## TEMPERATURE DEPENDENT SWITCHING BEHAVIOR OF BFN THIN FILMS: A WIDE BAND GAP SEMICONDUCTOR

*Devang D. Shah*<sup>1</sup>, *P.K. Mehta*<sup>1</sup>, *M.S. Desai*<sup>2</sup>, *C.J. Panchal*<sup>2</sup>

<sup>1</sup> Department of Physics, Faculty of Science,  
The M. S. University of Baroda, 390002, Vadodara, India  
E-mail: [devangshah\\_04@yahoo.co.in](mailto:devangshah_04@yahoo.co.in)

<sup>2</sup> Applied Physics Department, Faculty of Technology and Engineering,  
The M. S. University of Baroda, 390001, Vadodara, India

*The thin film of complex perovskite  $Ba(Fe_{0.5}Nb_{0.5})O_3$  (BFN) was prepared through Pulsed Laser Deposition (PLD) technique. XRD and AFM studies show single cubic phase with well developed nano size grains of BFN compound. Swift Heavy Ion (SHI) irradiation on BFN of  $O^{+7}$  ions up to  $1 \times 10^{13}$  ions per cc fluence does not show any crystal or morphological structural changes in the film, signifying materials stability up to the above ion dose. BFN compound exhibit its band gap in wide band semiconductor region (3.53 eV). A characteristic negative temperature co-efficient of resistance (NTCR) to positive temperature co-efficient of resistance (PTCR) transition of large magnitude at  $\sim 350$  °C makes BFN a promising candidate for electrical/magnetic switching device.*

**Keywords:** X-RAY DIFFRACTION, ATOMIC FORCE MICROSCOPY, PLD THIN FILMS, ION IRRADIATION EFFECTS, WIDE BAND GAP SEMICONDUCTOR.

(Received 04 February 2011, in final form 29 April 2011)

### 1. INTRODUCTION

The complex ceramic compounds having double perovskite structure have wide area of application due to their wide functional properties like; ferroelectricity, magneto electric behavior, relaxor properties, multiferroic behavior, piezoelectricity etc [1-5]. The increasing demand of miniaturization requires thin film preparation of such compounds. The Pulsed Laser Deposition (PLD) technique is one of the most promising ways to prepare thin films of such complex perovskite compounds. In addition electronic device industry requires environment friendly material. The Barium (Ba), Strontium (Sr) and Bismuth (Bi) are found most prominent candidates for replacement of toxic Lead (Pb) based compounds. Among these environment-friendly materials Barium based  $Ba(Fe_{0.5}Nb_{0.5})O_3$  (BFN) is widely studied material due to its promising electrical and magnetic properties [3, 6-8]. Preparations of thin films of BFN from the application point of view have been reported [9, 10]. N. Rama et.al. reported BFN thin film synthesis using PLD technique grown on  $LaAlO_3$  (LAO),  $NdGaO_3$  (NGO) and  $SrTiO_3$  (STO) substrates and their magnetic and transport properties are studied below room temperature region [9]. Later on, W. Zhang et.al. reported ferroelectric properties at room temperature of BFN films on Pt/TiO<sub>2</sub>/SiO<sub>2</sub>/Si substrate prepared using PLD [10]. They also highlighted on synthesis parameter dependent film

properties. To the best of our knowledge so far no one has studied structural and electrical properties of BFN films in the high temperature region with conducting substrate Indium Tin Oxide (ITO). The ITO coated glass substrate is found to be a suitable conducting substrate due to its wide availability, good conductivity and good lattice constant matching [11-12].

In the present work we synthesized BFN thin films using PLD technique on ITO coated glass substrate. The effect of Swift Heavy Ion (SHI) irradiation on structure and microstructure are reported here. Further the SHI irradiation effect on technologically important NTCR-PTCR transition up to high temperature region (up to 450 °C) is discussed from the application point of view.

## 2. EXPERIMENTAL

Thin films of complex ceramic compound BFN were deposited by Pulsed Laser Deposition (PLD) technique. Indium tin oxide (ITO) coated glass was utilized as conducting substrate. The bulk target of BFN ceramic was synthesized in pure single phase by conventional solid state reaction technique [13]. The well sintered disk of 25 mm diameter and 4 mm thickness was utilized as PLD target. The substrate was mounted at 3.5 cm from the target after ultrasonic cleaning for 10 min with acetone and then methanol. The laser source of 248 nm wavelength and 220 mJ energy with repetition rate of 10 Hz was utilized for deposition. The deposition chamber was evacuated down to a base pressure of  $1 \times 10^{-5}$  torr before deposition. The deposition was carried out at 400 °C with oxygen partial pressure of 250 m torr for 40 minutes. After deposition the chamber was completely filled with the oxygen and then cooled down to room temperature. The As deposited films were annealed in air atmosphere at 600 °C up to 1 hour for better crystallinity [14]. The SHI irradiation study was performed using pelletron accelerator at IUAC, New Delhi. For irradiation the films were mounted on a copper target ladder using silver paste inside a vacuum of  $1 \times 10^{-6}$  torr. Films were irradiated at room temperature using  $O^{+7}$  ions having energy of 98 MeV for three different fluences viz.  $1 \times 10^{12}$ ,  $5 \times 10^{12}$  and  $1 \times 10^{13}$  ions per  $cm^2$ . The structural properties and surface morphologies of pristine film (BFN-2P) along with irradiated films BFN-2A (fluence  $1 \times 10^{12}$  ions per  $cm^2$ ), BFN-2B (fluence  $5 \times 10^{12}$  ions per  $cm^2$ ), and BFN-2C (fluence  $1 \times 10^{13}$  ions per  $cm^2$ ) were studied using XRD and AFM measurements. X-ray diffraction measurements were done at CSR Indore, using Bruker D8 advance X-ray diffractometer. The x-rays were produced using a sealed tube and the wavelength of x-ray was 0.154 nm (Cu K-alpha). The x-rays were detected using a fast counting detector based on Silicon strip technology (Bruker LynxEye detector). The surface images of all the films were collected using AFM measurements. The UV-Vis spectroscopic measurements of the films were done at room temperature in the range of 300 nm to 850 nm. Further, the electrical characterization of films were done using SOLARTRON 1260 impedance analyzer in the frequency range of 1 Hz to  $1 \times 10^7$  Hz with temperature variation from 20 °C to 450 °C.

### 3. RESULTS AND DISCUSSION

#### 3.1 Crystal structure and microstructure analysis

The XRD patterns of pristine film (BFN-2P) and irradiated films (BFN-2B and BFN-2C) along with bulk target BFN and ITO substrate are shown in the Fig. 1.

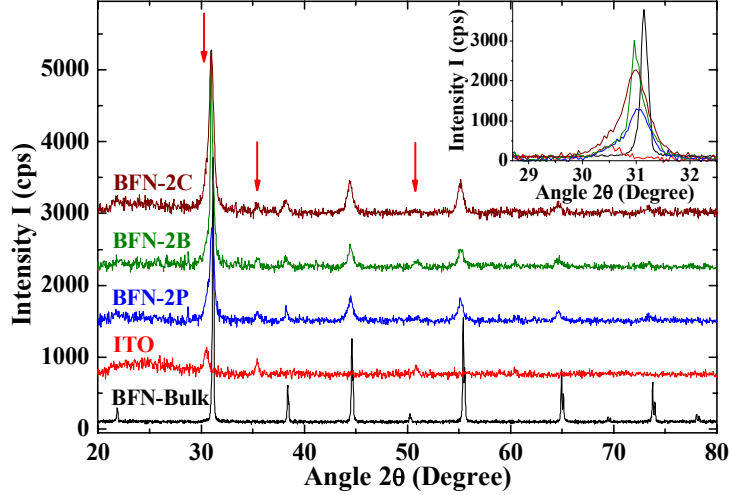


**Fig. 1** – The XRD pattern of BFN-Bulk target, ITO substrate, pristine thin film (BFN-2P), film irradiated at fluence  $5 \times 10^{12}$  ions per  $\text{cm}^2$  (BFN-2B) and film irradiated at fluence  $1 \times 10^{13}$  ions per  $\text{cm}^2$  (BFN-2C). (All patterns are uplifted by 750 cps from the below pattern except BFN-Bulk). Inset shows the distinct peaks belonging to sample and ITO

It is revealed from the Figure 1 that single cubic phase related to BFN is observed in each of these thin film samples. The peaks marked by vertical downward arrow are due to the ITO substrate. The space group  $p_m3_m$  with lattice parameter  $4.06 \text{ \AA}$  reported for bulk material by us [13] remains unchanged for each of the films irrespective of different irradiation fluences. This indicates that there is no significant crystallographic structural change has occurred up to above mentioned irradiation of  $\text{O}^{+7}$  ions on the thin films. The inset graph of Figure 1 clearly demonstrates the distinct peaks belonging to sample and ITO.

The quantitative analysis of XRD data in terms of strain broadening and crystallite size is done using Williamson – Hall equation [15] given by;

$$\beta \cos \theta = \frac{0.9\lambda}{L} + 4\varepsilon \sin \theta, \quad (1)$$

This equation distinguishes the strain broadening and broadening due to crystallite size. The plot between  $\beta \cos \theta$  and  $\sin \theta$  gives a straight line having intercept  $0.9\lambda/L$  and slope  $4\varepsilon$ . The values of crystallite size  $L$  and strain  $\varepsilon$  can be determined using intercept and slope of the graph respectively. Here  $\beta$  is FWHM determined from the XRD pattern,  $\theta$  is Bragg angle and  $\lambda$  is wave length of X-rays used. Figure 2 shows such Williamson – Hall plot for

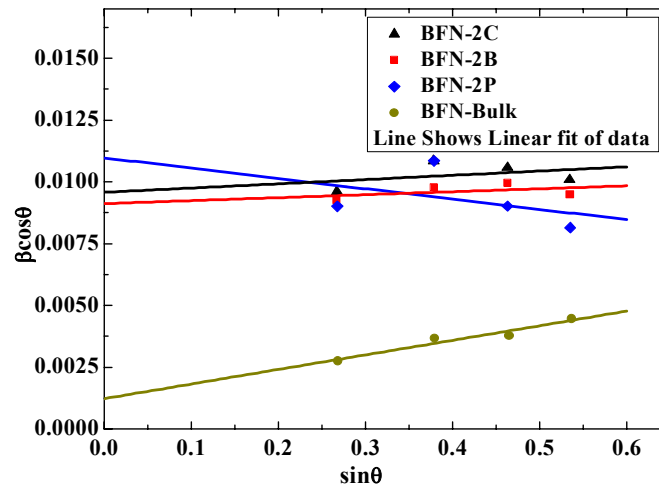


**Fig. 2** – Williamson-Hall plot for BFN-Bulk target, pristine thin film (BFN-2P), film irradiated at fluence  $5 \times 10^{12}$  ions per  $\text{cm}^2$  (BFN-2B) and film irradiated at fluence  $1 \times 10^{13}$  ions per  $\text{cm}^2$  (BFN-2C)

films along with bulk target. It is clear from the intercept values that crystallite size for films ( $\sim 13$  nm) is much smaller than the bulk target ( $\sim 113$  nm). The values of crystallite size and strain are listed in table 1. The very small values of strain ( $\sim 1 \times 10^{-3}$ ) indicates that there is no significant broadening due to strain on the XRD pattern. The observed negative value for pristine BFN film indicates nearly strain less growth of films [16]. Further, the values of the crystallite size do not show any unidirectional nature. The crystallite size is highest for BFN-2b film with irradiation fluence of  $5 \times 10^{12}$  ions per  $\text{cm}^2$ .

**Table 1** – Structural and Micro structural parameters calculated from XRD and AFM analysis

Sample	XRD		AFM				
	Strain $\times 10^{-3}$	Crystallite Size (nm)	RMS Roughness (nm)	Average Roughness (nm)	Height of Maximum Available Peak (nm)	Maximum Valley Depth (nm)	Maximum Peak Height (nm)
BFN-Bulk	1.48	112.9	–	–	–	–	–
BFN-2P	-1.04	12.6	20.02	15.75	42.53	74.00	40.70
BFN-2B	0.30	15.2	17.54	13.58	35.66	70.26	40.26
BFN-2C	0.43	14.5	16.78	13.34	35.16	64.84	34.28

The microstructure analyses of the films were done by AFM measurement. Figure 3 shows 2D and 3D AFM images of respective film surfaces. It is seen from the images that clusters of grains with well defined grain boundaries are observed. Detailed processing of the images was done in the

light of roughness parameters and particle height. The rms roughness and average roughness are listed above in Table 1. The surface roughness of the films is found decreasing with increase in the irradiation fluence. The surface roughness histogram is shown in the Figure 4. The height of maximum available peak is determined using histogram analysis. The results (Table 1) show that average available particle size decreases with increase in irradiation fluence. These results are not in accordance with the variation in the crystallite size from the XRD analysis. It means that because of irradiation the particle size reduces but the crystallinity improves than that of pristine film. The crystallinity increases up to fluence  $5 \times 10^{12}$  ions per  $\text{cm}^2$  and then reduces with higher fluence. The maximum peak height and maximum valley depth were determined from the average surface line (Table 1).

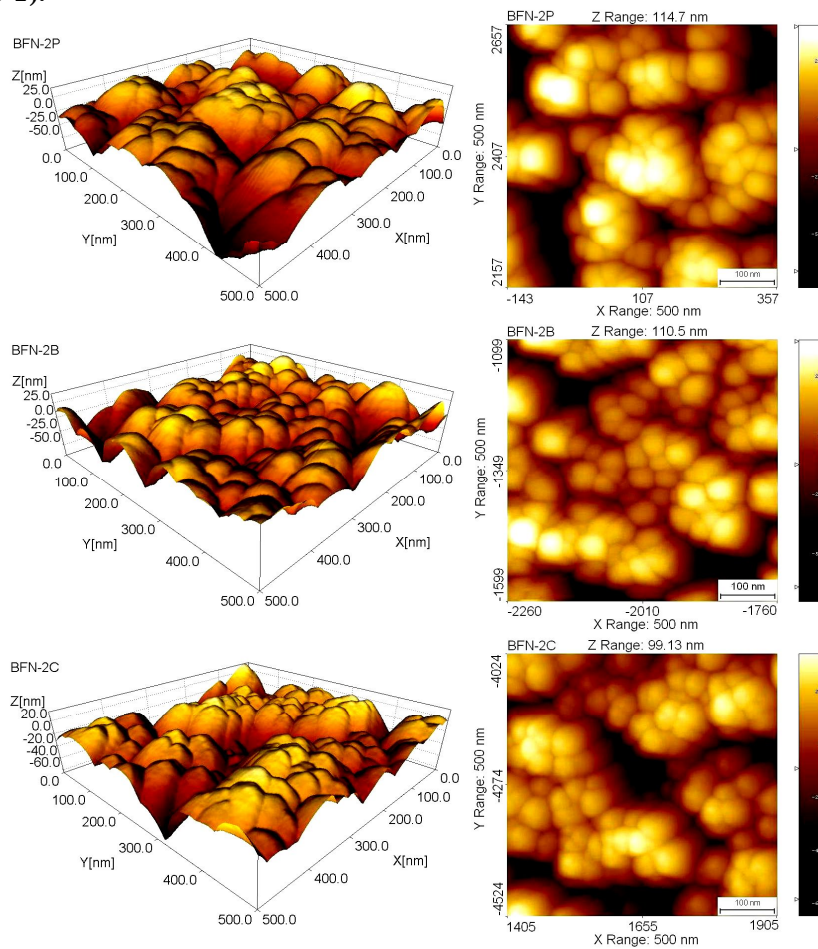


**Fig. 3** – 3-D and 2-D images of pristine thin film (BFN-2P), film irradiated at fluence  $5 \times 10^{12}$  ions per  $\text{cm}^2$  (BFN-2B) and film irradiated at fluence  $1 \times 10^{13}$  ions per  $\text{cm}^2$  (BFN-2C) collected using AFM

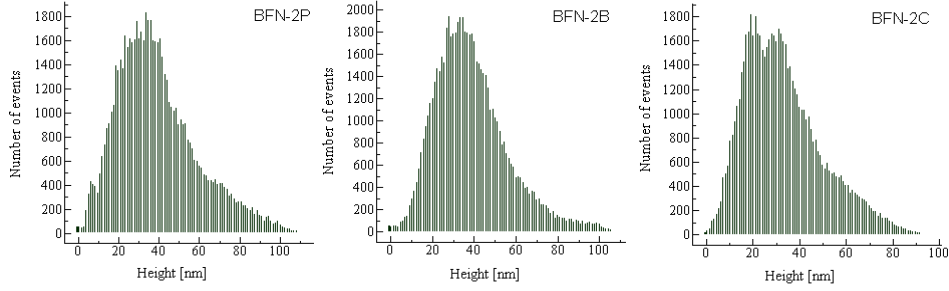


**Fig. 4** – Roughness histogram showing peak height statistics for pristine thin film (BFN-2P), film irradiated at fluence  $5 \times 10^{12}$  ions per  $\text{cm}^2$  (BFN-2B) and film irradiated at fluence  $1 \times 10^{13}$  ions per  $\text{cm}^2$  (BFN-2C)

It is to be noted here that the particle size determined using AFM are higher than the crystallite size determined using XRD. It means that the particles observed in the AFM images are not single crystals but are made-up of few crystallites. The micro structure along with the crystal structure analysis again indicates that no significant change has occurred up to the fluence of  $1 \times 10^{13}$  ions per  $\text{cm}^2$  irradiation of  $\text{O}^{+7}$  ions on the BFN thin films.

### 3.2 Optical analysis

The optical characterization of the pristine thin film was performed by UV-vis transmittance measurements. The optical absorption coefficient,  $\alpha$ ; can be calculated from the transmittance using the formula:

$$\alpha = \frac{1}{d} \ln \left( \frac{1}{T} \right), \quad (2)$$

where,  $d$  is thickness of the sample and  $T$  is the transmittance. The relation between optical band gap energy  $E_g$  and absorption co-efficient  $\alpha$  can be given by well-known Davis and Mott equation [17]:

$$\alpha h\nu = \left[ D (h\nu - E_g) \right]^\gamma, \quad (3)$$

where, constant  $D$  is the edge width parameter. The parameter  $\gamma$  depends on the type of transition occurs in the material. In order to calculate activation energy values the plot between  $(\alpha h\nu)^{1/\gamma}$  and  $h\nu$ , generally known as Tauc plot [12, 18], is shown in the Figure 5 with  $\gamma = 0.5$  for direct allowed transition.

Extrapolating the linear parts of the Tauc plot (with  $\gamma = 0.5$ ) gives a direct band gap  $E_g$  of 3.53 eV for the pristine film. The band gap value falls under the category of wide band gap semiconductor range. The observed oscillating value for transmittance in the inset graph is likely due to the interference effects. Similar oscillations were reported when transparent thin films are deposited on transparent substrates [19-20].

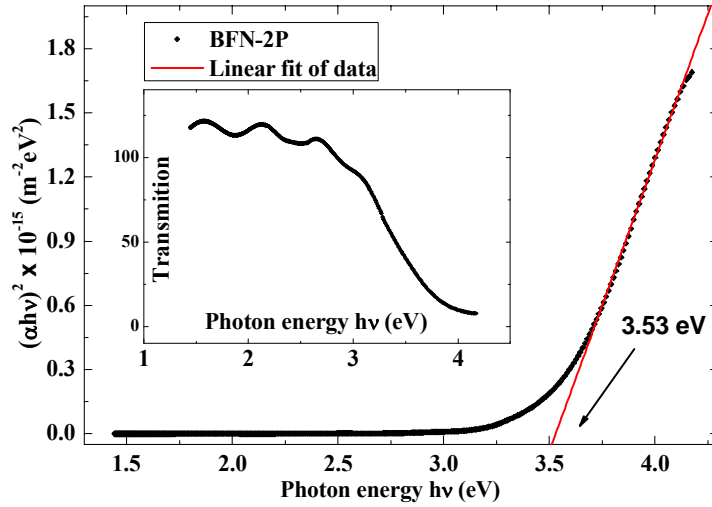


*Fig. 5 – Tauc plot for pristine thin film (BFN-2P) obtained using UV-VIS transmittance data. Inset shows oscillations in transmittance data*

### 3.3 RESISTIVITY ANALYSIS

The variation of resistivity with temperature for above films at 1 kHz frequency is shown in Figure 6. It is observed that overall resistivity decreases with increase in the irradiation fluences. The decrease in resistivity points towards development of defects like oxygen vacancies in the films due to the enhanced surface to bulk ratio resulting from smaller crystallite size. Defects of such kind increase the carrier concentration of electrons and holes.

In general temperature dependent resistivity can be given by Arrhenius equation:

$$\rho = \rho_0 \exp\left(\frac{E_a}{kT}\right), \quad (4)$$

Here,  $\rho_0$  is resistivity at infinite temperature,  $E_a$  is activation energy,  $k$  is Boltzmann constant and  $T$  is absolute temperature. This equation suggests monotonic logarithmic nature of resistivity data. In the present case resistivity decreases with increases in temperature up to 350 °C showing normal semi-conducting behavior of the films, this could be explained using above equation. But, for the temperatures above 350 °C resistivity makes a valley and starts increasing with temperature. This typical nature of films indicates metal like conduction in the films. Such change in the nature of resistivity curve points towards presence of a phase transition. It may also be due to possible change in the mechanism of conduction. During such transition the activation energy values do not remain constant. Hence such behavior of resistivity could not be explained by Arrhenius equation. For further analysis of such unanticipated resistivity data we calculated temperature dependent activation energies using derivative equation [13, 21]:

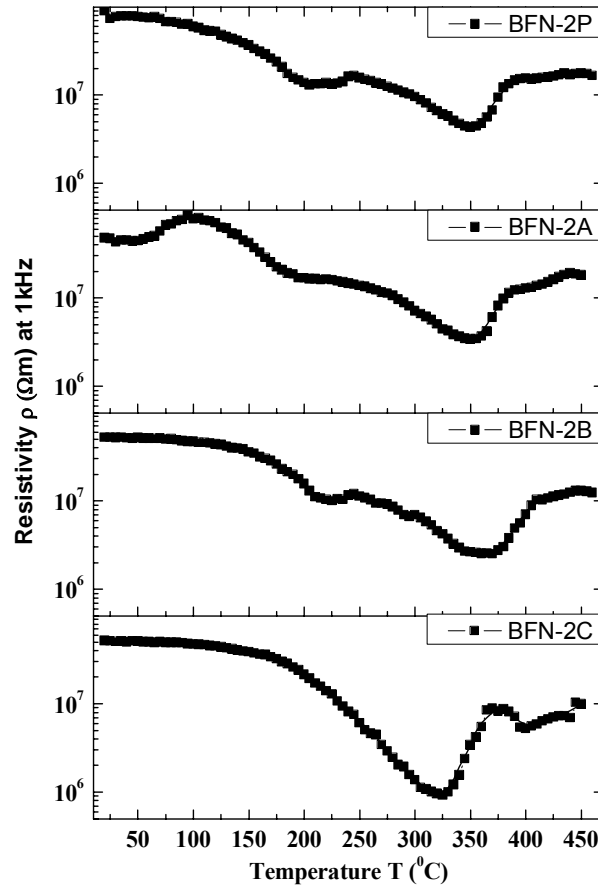


**Fig. 6** – Temperature dependent resistivity data of pristine thin film (BFN-2P), film irradiated at fluence  $1 \times 10^{12}$  ions per  $\text{cm}^2$  (BFN-2A), film irradiated at fluence  $5 \times 10^{12}$  ions per  $\text{cm}^2$  (BFN-2B) and film irradiated at fluence  $1 \times 10^{13}$  ions per  $\text{cm}^2$  (BFN-2C) at 1 kHz frequency

$$E_a = k \frac{d \ln \rho}{d(1/T)}, \quad (5)$$

In addition the temperature co-efficient of resistance (generally abbreviated as  $\alpha$  but here to distinguish with optical absorption coefficient abbreviated as TCR) is also very useful tool for such investigation along with temperature dependent activation energy analysis. The TCR can be calculated from the resistivity data using following equation [22]:

$$\text{TCR} = \frac{1}{R} \frac{dR}{dT} = \frac{1}{\rho} \frac{d\rho}{dT}, \quad (6)$$

Figure 7a and 7b shows, respectively, temperature dependent activation energy values and TCR values for each of the thin film samples. It is clear

from the graph that the activation energies  $E_a$  remain constant in the region near to room temperature. The typical low values  $\sim 0.1$  eV suggests that the conduction in this region is dominated by the free charge carriers like electrons trapped at singly ionized oxygen vacancies [23-25]. On increasing the temperature from room temperature to 200 °C, the singly ionized oxygen vacancies makes a transition to doubly ionized oxygen vacancies. This is reflected through increase in activation energy to  $\sim 0.5$  eV.

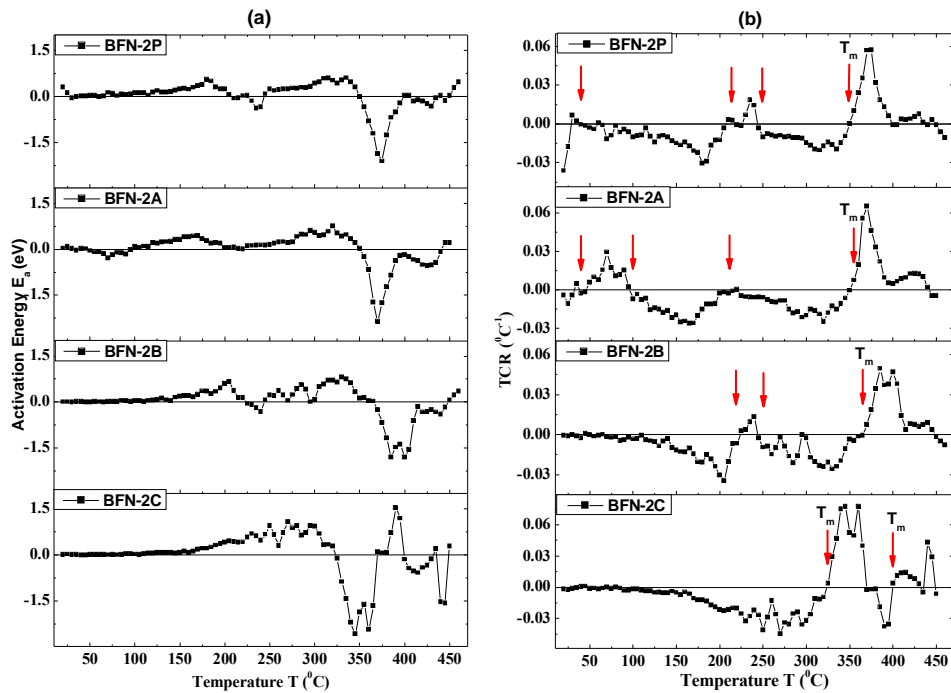


**Fig. 7** – Temperature dependent activation energy values (a) and temperature dependent TCR values for pristine thin film (BFN-2P), film irradiated at fluence  $1 \times 10^{12}$  ions per  $cm^2$  (BFN-2A) (b), film irradiated at fluence  $5 \times 10^{12}$  ions per  $cm^2$  (BFN-2B) and film irradiated at fluence  $1 \times 10^{13}$  ions per  $cm^2$  (BFN-2C)

A normal behavior of semi conducting thin films is to show negative temperature co-efficient of resistance (NTCR) where as metallic behavior is linked to positive temperature co-efficient of resistance (PTCR). In BFN film samples, up to 300 °C, we observe a number of transitions between NTCR-PTCR. Higher dose of SHI irradiation using  $O^{+7}$  on BFN films suppress such NTCR-PTCR transitions. The observed behavior points that the origin of these transitions is purely due to local variation in the defects. But in contrast a strong NTCR-PTCR transition at 350 °C could not be eliminated by means of SHI irradiation of  $O^{+7}$  in BFN films. The transition found splitted in to two for highest fluence of  $O^{+7}$ . Similar variation is observed for the  $E_a$  values also. In addition the activation energy values decreases sharply up to  $\sim -2.0$  eV and again sharply rises to positive values. These results clearly suggest that the transition observed at  $\sim 350$  °C is not only related with the changes in the conduction mechanism but it is also related with a structural

transition linked electrical or magnetic phase transition. The observed sudden transition and its temperature variations with irradiation fluence can be effectively used to prepare electrical/magnetic switching semi-conducting device. Exact nature requires further investigations.

#### 4. CONCLUSION

In BFN films, with single cubic phase, the crystallite size drastically falls to ~ 13 nm compared to bulk (~ 113 nm). Over all crystal structure and micro structure of BFN film remains nearly unaffected up to the fluence of  $1 \times 10^{13}$  ions per  $\text{cm}^2$  SHI irradiation using  $\text{O}^{+7}$ . The BFN bulk and its thin films, deposited on ITO coated glass substrate, exhibit band gap in wide band semiconductor region. A prominently large NTCR to PTCR transitions at 350 °C whose origin is a temperature dependent structure linked electrical/magnetic phase transition rather than a local fluctuating defects makes BFN film a promising candidate as switching device. Further, the switching temperature can also be modified using appropriate SHI irradiation fluence.

We are thankful to UGC-DAE CSR (India), for providing measurement facilities at Indore centre.

#### REFERENCES

1. Y. Shimakawa, M. Azuma, N.I. Chikawa, *Materials* **4**, 153 (2011).
2. D. Serrate, J.M.De Teresa, M.R. Ibarra, *J. Phys.: Condens. Matter* **19**, 023201 (2007).
3. Z. Wang, X.M. Chen, L. Ni, X.Q. Liu, *Appl. Phys. Lett.* **90**, 022904 (2007).
4. J.V.D. Brink, D.I. Khomskii, *J. Phys.: Condens. Matter* **20**, 434217 (2008).
5. M.G. Blamire, J.L. MacManus-Driscoll, N.D. Mathur, Z.H. Barber, *Adv. Mater.* **21**, 3827 (2009).
6. I.P. Raevski, S.A. Prosandeev, A.S. Bogatin, M.A. Malitskaya, L. Jastrabik, *J. Appl. Phys.* **93**, 4130 (2003).
7. Z. Wang, X.M. Chen, L. Ni, X.Q. Liu, *Appl. Phys. Lett.* **90**, 022904 (2007).
8. N. Rama, J.B. Philipp, M. Opel, K. Chandrasekaran, V. Sankaranarayanan, R. Gross, M.S.R. Rao, *J. Appl. Phys.* **95**(11), 7528 (2004).
9. N. Rama, J.B. Philipp, M. Opel, V. Sankaranarayanan, R. Gross, M.S.R. Rao, *J. Phys. D: Appl. Phys.* **40**, 1430 (2007).
10. W. Zhang, L. Li and X.M. Chena, *J. Appl. Phys.* **106**, 104108 (2009).
11. M.D. Benoy, E.M. Mohammed, S. Babu M., P.J. Binu, B. Pradeep, *Braz. J. Phys.* **39**(4), 629 (2009).
12. M.H. Habibi and N. Talebian, *Acta Chim. Slov.* **52**, 53 (2005).
13. D.D. Shah, P.K. Mehta, M.S. Desai, C.J. Panchal, *J. Alloys Comp.* **509**, 1800 (2011).
14. S.T. Tan, B.J. Chen, X.W. Sun, W.J. Fan, H.S. Kwok, X.H. Zhang, S.J. Chua, *J. Appl. Phys.* **98**, 013505 (2005).
15. G.K. Williamson, W.H. Hall, *Acta Metall.* **1**, 22 (1953).
16. S. Pratapa, B. O'Connor, *Adv X-ray Anal.* **45**, 41 (2002).
17. E.A. Davis, N.F. Mott, *Philos. Mag.* **22**, 903 (1970).
18. J. Tauc, *Mater. Res. Bull.* **5**, 721 (1970).
19. R. Swanepoel, *J. Phys. E: Sci. Instrum.* **16**, 1214 (1983).
20. C. Mansilla, *Solid State Sci.* **11** 1456 (2009).
21. J. Jadzyn, D. Baumen, J.-L. Dejardin, M. Ginovska, G. Czechowski, *Acta Phys. Pol. A* **108**, 479 (2005).

22. J.L. Wang, Y.S. Lai, S.C. Liou, C.C. Tsai, B.S. Chiou, H.C. Cheng, *J. Phys. D: Appl. Phys.* **41**, 085304 (2008).
23. C. Ang, Z. Yu, L.E. Cross, *Phys. Rev. B* **62**, 228 (2000).
24. II-Doo Kim, A. Rothschild and H. L. Tuller *Appl. Phys. Lett.* **88**, 072902 (2006).
25. W.H. Han, X.K. Chen, E.Q. Xie, G. Wu, J.P. Yang, R. Wang, S.Z. Cao, Y.L. Wang, *Surf. And Coat. Tech.* **201**, 5680 (2007).